Publication III

R. C. D. Paiva, J. Pakarinen, V. Välimäki, and M. Tikander. Real-time audio transformer emulation for virtual tube amplifiers. *EURASIP J. Advances Signal Processing*, **pp. 1–15, Feb. 2011.**

Research Article

Real-Time Audio Transformer Emulation for Virtual Tube Amplifiers

Rafael Cauduro Dias de Paiva,[1, 2] Jyri Pakarinen,[1] Vesa Välimäki,[3] and Miikka Tikander[3]

[1] *Department of Signal Processing and Acoustics, School of Electrical Engineering, Aalto University, 02150 Espoo, Finland*
[2] *Nokia Institute of Technology (INdT), SCS 1 Ed. Camargo Corrêa, 6th floor, 70397900 Brasilia, Brazil*
[3] *Nokia Gear, Itämerenkatu 11, 00180 Helsinki, Finland*

Correspondence should be addressed to Rafael Cauduro Dias de Paiva, rcdpaiva@yahoo.com.br

An audio transformer is used in a guitar amplifier to match the impedances of the power amplifier and a loudspeaker. It is important to understand the influence of the audio transformer on the overall sound quality for realistic tube amplifier emulation. This paper proposes to simulate the audio transformer using a wave digital filter model, which is based on the gyrator-capacitor analogy. The proposed model is two-directional in the sense that it outputs the loudspeaker current, but it also connects backward to the power amplifier thus affecting its behavior in a nonlinear manner. A practical parameter estimation procedure is introduced, which requires only the measurement of basic electrical quantities but no knowledge of material properties. Measurements of a Fender NSC041318 and a Hammond T1750V transformer are presented as case studies, as well as parameter fitting and simulation for the Fender transformer. The results show that these practical transformer designs introduce distortion at low frequencies only, below about 100 Hz for the Fender and 30 Hz for the Hammond transformer, and that the proposed model faithfully reproduces this effect. The proposed audio transformer model is implemented in real time using the BlockCompiler software. Parametric control allows varying and also exaggerating the model nonlinearities.

1. Introduction

Although there are new and cheaper technologies for guitar effects and amplification, vacuum tube amplifiers remain extremely popular. Some reasons for this popularity are the soft clipping characteristics of tubes, which nicely enhance guitar timbre, and also that many guitar players strive for the same sound as their idols from the 60s and 70s. Despite their nice sound characteristics, vacuum tube amplifiers rely on heavy and bulky components, and they typically are much more expensive than their solid-state counterparts.

Audio transformers represent an important part of guitar power amplifiers. They are responsible for the impedance matching between amplification circuits and the loudspeaker, but they also have an effect on the amplified signal. Audio transformers by themselves do not have a flat frequency response. This is caused by the magnetizing inductance, parasitic reactances, such as leakage inductance,

winding capacitances, and by frequency-dependent losses present in magnetic components. These losses include ohmic losses, caused by winding resistances; eddy current losses, caused by parasitic currents induced in the magnetic material due to varying magnetic flux; hysteresis losses. The latter two are caused by the fact that magnetic materials change their behavior every time the magnetic flux is reversed causing a small amount of energy to be dissipated at every cycle, resulting in frequency-dependent losses. Additionally, the magnetic material in audio transformers may present a frequency-dependent saturation, which differs significantly from the saturation caused by vacuum tube amplifier stages.

Many studies have been performed in recent years on the emulation of vacuum tube amplifiers [1], which are often implemented in low-cost guitar effects. Some popular approaches derive from static waveshaping, which does not simulate the nonlinear dynamics of the full amplification system. Additionally it is possible to use nonlinear filters,

such as Volterra techniques [2], which can be matched to the desired nonlinear response characteristic, and physics-based approaches, which are chosen for this work. Among physical modeling techniques, some works focus on directly modeling and solving the differential equations of the nonlinear circuits [3–5], nodal analysis and state-space approaches [6, 7], and wave digital filters (WDFs) [8–11]. WDFs provide a simple approach for circuit emulation, which enables efficient implementation in real time.

Audio transformer models in the literature include linear models implemented in SPICE [12], WDFs [10], extended state-space techniques [13], and differential equation approximation [14]. Additionally, a nonlinear model for offline vacuum tube guitar simulation is proposed in [15] using the Jiles and Atherton model [16] for magnetic losses. Different models for magnetic behavior are available in the literature. The Jiles and Atherton model includes implicit differential equations used to determine the behavior of magnetic hysteresis. This is successful for modeling magnetic behavior, although parameter fitting may not be straightforward, and the concept complexity tends to push designers/engineers to simpler solutions. A hyperbolic curve fitting procedure is proposed in [17], where the function can be easily fitted by parameters available in magnetic material datasheets. However, the determination of the curve shape is based on flux maximum and minimum values and would need to be dynamically changed as the waveform varies. This is usually not a problem for power electronics simulations in which the signal amplitude and frequency are kept nearly constant but would be for audio signals, which have a wide bandwidth and varying amplitudes.

Other models have emerged from the gyrator-capacitor (GC) analogy, which provides an intuitive approach for understanding magnetic behavior [18]. This approach makes understanding the behavior of highly complex magnetic circuits possible [19], and a complete model including core saturation and hysteresis may be obtained with a nonlinear capacitor and resistor [20]. Additionally, the elements used in this model make it an excellent candidate for implementation using WDFs. Preisach and other multistate transformer models [21] are cumbersome and costly and may not be appropriate for real-time implementation. Therefore, the GC model was chosen.

This paper proposes a WDF implementation of a nonlinear audio transformer model for real-time guitar amplifier emulation. The complete model for audio transformer includes, in addition to the nonlinear transformer behavior, parasitic phenomena such as leakage inductance, winding resistance, and input/output capacitance, which are important for matching the transformer's frequency response. Nonlinear behavior is modeled using a GC approach [20], and a parameter fitting procedure is proposed requiring only simple measurements instead of prior knowledge of material properties, since in many cases detailed information is not available for the material and core type. A WDF model is proposed to enable realistic simulation of the interaction between the transformer's varying impedance and the backward connected circuitry, which changes its distortion behavior with the nonlinear load represented by

the transformer. A real-time implementation of a complete output chain of a single-ended guitar amplifier is described, which proves the feasibility of the method.

Section 2 reviews some basic concepts of transformer behavior, as well as magnetic quantities. A short introduction on WDFs is presented in Section 3, focusing on the implementation aspects used in this paper. Section 4 presents the transformer model using the GC approach, while Section 4.2 presents a new fitting procedure for the proposed model. In Section 4.3 a new WDF implementation of the audio transformer is presented. In Section 4.4 a measurement setup is proposed for parameter fitting and testing the proposed model, while in Section 4.5 simulated and measurement results are compared. In Section 5 the proposed model is included in the output chain of a single-ended vacuum tube amplifier implemented in real time using WDFs. Section 6 concludes the paper.

2. Transformer Characteristics and Nonlinearity

The nonlinear behavior of an audio transformer has some peculiar characteristics which differ from other components in vintage analog circuits. Since saturation-like distortion occurs in the magnetic domain, it does not manifest itself as simple clipping in the electrical domain. Additionally, magnetic distortion is dependent on previous values of the magnetic field, and the distortion cannot be modeled with simple static nonlinearities.

Electrical signals are related to magnetic signals by the following well-known relationships. The voltage E is the time derivative of the magnetic flux Φ,

$$E = \frac{-N\mathrm{d}\Phi}{\mathrm{d}t};\qquad(1)$$

where N is the number of turns. The magnetic flux is related, in turn, to the magnetic field, or flux density, B by the area integral

$$\Phi = \int B\mathrm{d}a = BA_{\mathrm{e}},\qquad(2)$$

where A_{e} is the core's effective area. The flux density B is most often used in magnetic material specifications, since magnetic properties using Φ are related to the transformer's core geometry. The magnetizing force H is related to the current flowing in a winding of a transformer by simply considering its number of turns N so that

$$H = Ni,\qquad(3)$$

where i is the current through the winding.

For linear magnetic materials, B is linearly related to H as

$$B = \mu H,\qquad(4)$$

where μ represents the permeability of the material. However, this relationship is not followed for high values of B or H,
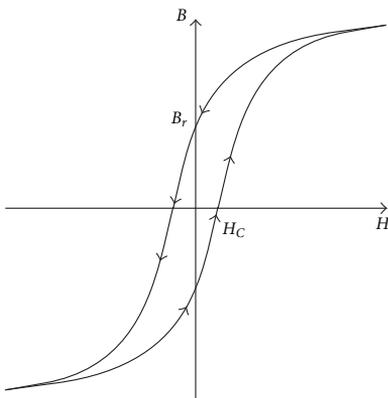
FIGURE 1: Basic theoretical B versus H curve showing hysteresis.

as shown in Figure 1, where it can be seen that, for high excursions in H, saturation occurs in B. This effect is caused by the inherent properties of magnetic materials, which can be interpreted as decreased permeability for high values of H. Additionally, a loop can be observed in the B versus H curve, which means that the B value not only depends on the H value but also on its previous magnetic history. This loop is related to losses occurring in the magnetic material which increases with frequency.

Figure 2(a) shows an example of how distortion would occur in an audio transformer. In this example assuming a 1 : 1 turns ratio, the output voltage would be expected to be the same as the input when no magnetic saturation takes place. Observing the 50 Hz example, shows that distortion occurs after the input voltage has reached its peak and lingers after the input voltage has begun to decrease. This happens because the magnetic flux Φ relates to voltage via a derivative operation, and hence for a sinusoidal input there is a 90 degree shift between the flux and voltage. As saturation occurs in the B versus H mapping, maximum B would be reached at a voltage near zero, where maximum distortion is observed.

The same transformer produces different saturation behavior at different frequencies for the same characteristics of the input signal. Figure 2(a) shows the expected behavior at 50 and 100 Hz. As can be observed, with doubled frequency almost no distortion is present in the output signal. As Φ is proportional to the integral of E in (1), it will have a higher amplitude when the frequency is lower. Additional input/output voltage relationships can be observed in Figure 2(c), where at 100 Hz a nearly linear relationship is seen, while it changes as frequency is decreased. The shape of the input/output mapping is also seen to change with frequency.

Thus, electric transformers have combined frequency-dependent losses and nonlinearity which causes them to have a bandpass characteristic. On one hand, high-frequency signals would have a small amount of nonlinear distortion and high magnetic losses. This frequency-dependent loss is related to the amount of energy transfer and will cause a decreased output voltage. On the other hand, although low-frequency signals would have lower magnetic losses, they would vanish from the high distortion caused by magnetic behavior.

In addition to the input/output voltage relationships, the impedance observed from input circuit changes when the transformer reaches saturation. As shown in Figure 2(b), a high current surge at the primary of the transformer is observed during saturation periods. In this period, the equivalent inductance in the primary winding is lower, and the coupling between the primary and the secondary is lower. Hence, the equivalent impedance in the primary is also lower, causing this kind of current surge. In guitar amplifier circuits, as shown in Figure 3, the series impedance of the primary connected to the valves will be lower at saturation, which will change the behavior of the amplifier circuit. Thus, the saturation of a transformer has an effect not only on its input/output relationship but it also modifies the behavior of the electronic components connected to it.

3. Wave Digital Filters

WFDs, introduced by Fettweis [22], offer a modular and relatively light approach for real-time circuit simulation. The main difference between WDFs and most other modeling methods is that WDFs represent all signals and states as wave variables and use local discretization for the circuit components instead of the physical quantities themselves. Different electrical components are represented as elementary blocks, and they are connected to each other via adaptor blocks. Only a brief introduction to WDFs is presented in the following. For more thorough tutorials, see, for example, [22, 23].

3.1. Wave Digital Filter Components. WDF components connect to each other using ports. Each port has two terminals, one for transporting incoming and another for transporting outgoing waves. Also, each port has an additional parameter, the port resistance, which is used to implement proper impedance coupling between components. The relationship between the Kirchhoff pair (e.g., voltage U and current I) and wave variables A and B is given by

$$\begin{bmatrix} A \\ B \end{bmatrix} = \begin{bmatrix} 1 & R_p \\ 1 & -R_p \end{bmatrix} \begin{bmatrix} U \\ I \end{bmatrix} \Longleftrightarrow \begin{bmatrix} U \\ I \end{bmatrix}$$
$$= \frac{1}{2} \begin{bmatrix} 1 & 1 \\ \dfrac{1}{R_p} & -\dfrac{1}{R_p} \end{bmatrix} \begin{bmatrix} A \\ B \end{bmatrix}, \tag{5}$$

where R_p denotes the port resistance.

It should be noted that this port resistance is purely a computational parameter and it should not be confused with the electrical resistance. Some elementary circuit components, such as resistors, capacitors, and inductors, can be represented using WDF one-port elements. Other electric components, such as transformers and gyrators, are represented with two-port elements. The linear electrical components used in this paper are presented together with
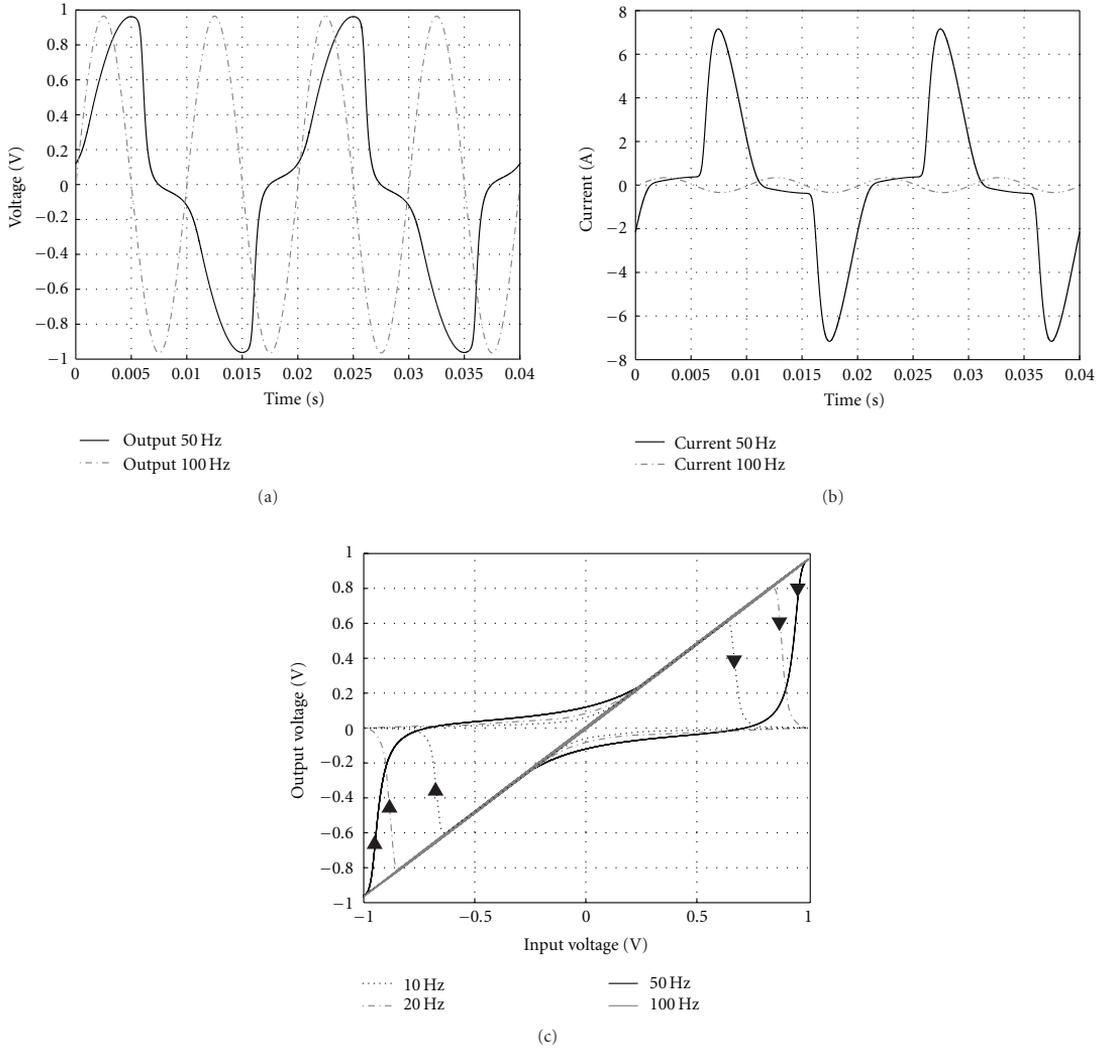
(a)

(b)

(c)

FIGURE 2: Example of saturation in a power transformer. (a) Output voltage and (b) current at 50 and 100 Hz and (c) the input versus output voltage.

their WDF counterparts in Figure 4. The port resistances of the one-port elements in Figure 4 can be given as follows:

$$R_{\mathrm{p}} = \begin{cases} R, & \text{for resistance,} \\ \dfrac{1}{(2CF_{\mathrm{s}})}, & \text{for capacitance,} \\ 2LF_{\mathrm{s}}, & \text{for inductance,} \end{cases} \qquad (6)$$

where $R, C,$ and L are the electrical resistance (Ohms), capacitance (Farads), and inductance (Henrys), respectively, while F_{s} stands for the sample rate (Hertz). Similar to the

WDF resistor, the port resistance of a voltage source is equivalent to the physical resistance. The port resistance of a gyrator is equal to its transformation ratio, and it is the same for both ports. The port resistances of a transformer are not identical but are related by the square of the turns ratio, as given in Figure 4(g).

3.2. Adaptors. The WDF circuit components connect to each other via adaptors. In practice, the adaptors direct signal routing inside the WDF circuit model and implement the correct impedance coupling via port resistances. Although the number of ports in an adaptor is unlimited in principle,
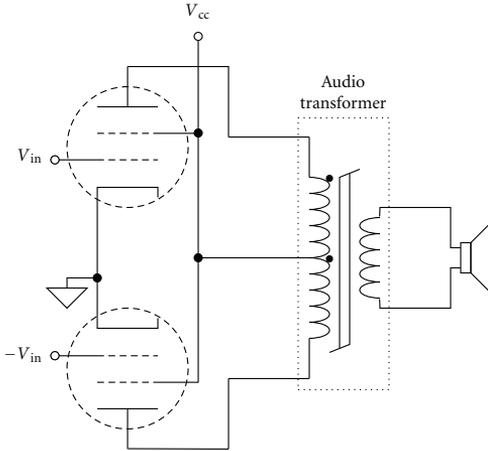
FIGURE 3: Typical guitar amplifier output stage using a push-pull topology.

3-port adaptors are typically used since any N-port adaptor ($N > 3$) can be expressed using a connection of 3-port adaptors so that the whole WDF circuit becomes a binary tree structure [24]. There are two types of WDF adaptors, series and parallel, which implement the series and parallel connection between elements, respectively. The port resistance values for the adaptors must be set equal to the port resistances of the elements they are connected to.

The outgoing wave B_n at port $n = 1, 2, 3$ of a 3-port adaptor can generally be expressed as

$$B_n = \begin{cases} \dfrac{A_n - 2R_n(A_1 + A_2 + A_3)}{(R_1 + R_2 + R_3)}, & \text{for a series adaptor,} \\[4mm] \dfrac{2(G_1A_1 + G_2A_2 + G_3A_3)}{(G_1 + G_2 + G_3) - A_n}, & \text{for a parallel adaptor,} \end{cases}$$

(7)

where A_n denotes the incoming wave at port n and $G_n = 1/R_n$ is the port conductance. Equation (7) shows that in principle all waves leaving the adaptor depend on all incoming waves and all port resistances. This poses a computability problem with such WDF components that have instantaneous dependencies between the port terminals, such as transformers, gyrators, and nonlinear components.

As a remedy, one WDF one-port component must be chosen as a root of the binary tree so that each simulation cycle starts by first evaluating the waves propagating towards the root after which the waves propagating away from the root are evaluated. This is enabled by properly selecting the adaptors' port resistances for the ports facing the root so that the waves traveling towards the root can be made independent of the waves traveling away from the root.

For example, if the port facing the root element is named as port one, and its port resistance is set to $R_1 = R_2 + R_3$ when it is a series adaptor, or its port conductance to $G_1 = G_2 + G_3$

when it is a parallel adaptor, then (7) simplifies to

$$B_1 = \begin{cases} -A_2 - A_3, & \text{for a series connection,} \\[4mm] \dfrac{G_2/(G_2 + G_3)A_2 + G_3}{(G_2 + G_3)A_3}, & \text{for a parallel connection,} \end{cases}$$

(8)

for the wave components traveling towards the root. In this example, port one would be called adapted, or reflection-free, since the outgoing wave does not depend on the incoming (reflected) wave. Such adapted ports are typically denoted by a "T-shaped" ending for the outward terminal.

3.3. Nonlinearities in WDFs. Nonlinear resistors can be modeled by defining the outgoing wave B as [25]

$$B = \frac{R - R_p}{R + R_p}A,$$

(9)

where R is the electrical resistance of the root, R_p is the port resistance set by the adapted port connected to the resistor, and A is the wave entering the resistor. Since the port resistance of the adapted port is independent of the electrical resistance of the root, the latter can freely be varied during simulation without encountering computability problems.

With nonlinear resistors, the resistance value depends on the voltage across the resistor, which in turn depends on the incoming and outgoing waves. As defined by (5) and (9), this creates an additional local implicit loop, which in principle should be solved iteratively. A practical remedy, however, is to insert a unit delay inside the loop. This approximation may affect stability under heavily saturating nonlinearities, but its effect is typically negligible under normal operating conditions (see, e.g., [11]).

Nonlinear electrical components can often be approximated using voltage-controlled voltage and current sources by reading the voltage across the source as the input signal, or by using an ideal variable-turns-ratio transformer connected to a constant element. The latter approach has the advantage of maintaining the energy balance when energy storing nonlinear elements are used. In the case of inductors and capacitors, the equivalent component value is easily determined by

$$L_e = \frac{L}{N^2},$$
$$C_e = CN^2,$$

(10)

where L and C are the original inductances and capacitance values, respectively, and N is the turns ratio of the time-varying transformer.

These circuit components also suffer from the above-mentioned local feedback loop, but artificial unit delays will usually solve this problem. Since a nonlinear WDF element should be connected as the root of the binary tree due to previously discussed computability issues, having multiple nonlinear components within a tree creates another problem. In principle, multiple nonlinearities would require global
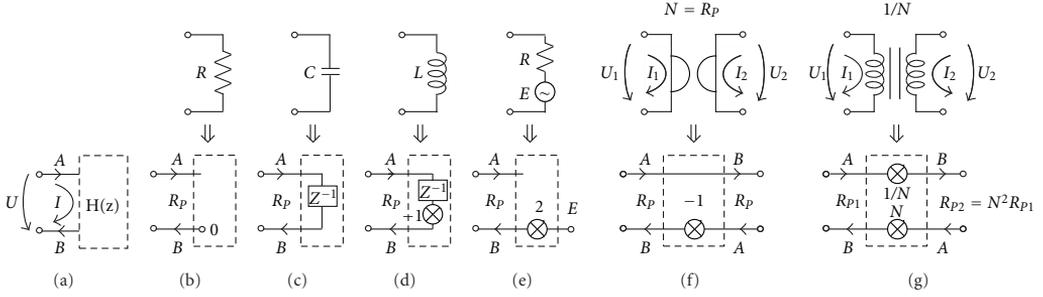
FIGURE 4: Linear WDF elements used in this paper: (a) a generic one-port with voltage U across and current I at the terminals, (b) a resistor, (c) capacitor, (d) inductor, (e) voltage source, (f) gyrator, and (g) an ideal transformer. Here, A represents an incoming wave for each element, while B denotes an outgoing wave. R_p stands for the port resistance. This figure is adapted from [11].
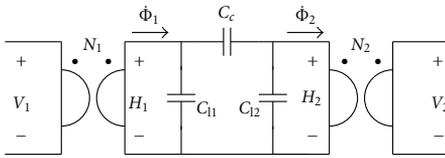

FIGURE 5: Basic gyrator-capacitor model of a transformer.

iteration on the subtree connecting the nonlinear elements, dramatically increasing the computational cost. As before, inserting a unit delay between the nonlinearities solves the computability issue but may create instabilities. As a general rule, by increasing the number of artificial unit delays, one increases the risk of encountering stability problems [26]. However, preliminary experimental tests suggest that, as long as the model stays stable, the unit delays do not result in audible artifacts.

4. Audio Transformer Model

4.1. Gyrator-Capacitor Model. The model used in this paper is based on a gyrator-capacitor (GC) approach [18]. This kind of model has been used in power electronics to model multiple-winding elements for its simplicity. By using this approach, the relationship between physical quantities can be easily visualized; hence, it also serves as a tool for understanding the magnetic behavior of the system.

A basic transformer model is shown in Figure 5. In this figure, gyrators, also known as dualizers, with transformation ratio N are used to model the conversion between electrical and magnetic quantities. The input/output relation of the gyrator is summarized by (11) and (12), which assures energy-conserving properties, since $v_1 i_1 = v_2 i_2$. Additionally, the gyrator interchanges the behavior of the capacitors/inductors and the current/voltage source:

$$v_1 = i_2 N, \tag{11}$$

$$i_1 = \frac{v_2}{N}. \tag{12}$$

By using the GC approach, the current and voltage in the electrical domain are related to the magnetizing force and magnetic flux in the magnetic domain by the same relations given in (1) and (3). The gyrator is used to convert the electrical quantities to the magnetic domain, where electrical voltage V is related to the magnetic flux density derivative $d\Phi/dt$ as in (1) and (11), and the electrical current I is related to the magnetizing force H as in (3) and (12), where N is the number of turns of the winding a gyrator is representing. In Figure 5, two windings with N_1 and N_2 turns are represented by the gyrators, and capacitances are related to possible magnetic paths, since (4) may be modified as

$$\Phi = BA_e = \mu H A_e, \tag{13}$$

$$\frac{d\Phi}{dt} = \mu A_e \frac{dH}{dt}, \tag{14}$$

where (14) can be interpreted as the equation of a capacitor with current $d\Phi/dt$, voltage H, and capacitance μA_e. In Figure 5, C_c represents the core permeance, which couples the primary and the secondary, while C_{l1} and C_{l2} represent the primary and secondary winding's leakage inductances, which model the uncoupled magnetic flux. Other parasitic elements may be included by adding series resistances R_1 and R_2 to each winding, representing the ohmic losses experienced by the transformer, and parallel capacitances C_1 and C_2, which affect the overall frequency response of the transformer.

The GC model can be extended by including a nonlinear capacitor, representing the core's nonlinear permeance [18], and a nonlinear resistor, modeling magnetic loss due to the hysteresis loop [20], as shown in Figure 6(a). By modification of the nonlinear capacitance C_c, it is possible to model the saturation effect in the B versus H curve. This model is often represented using a capacitor in series with a voltage-controlled voltage source, with the voltage $E_C(v_c)$ defined as

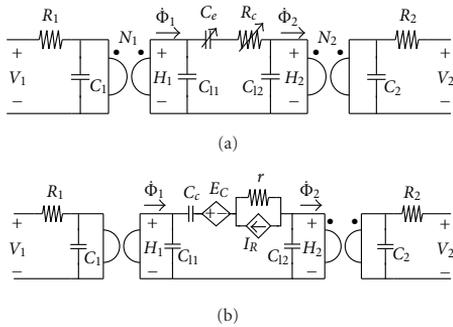$$E_C(v_c) = a|v_c|^n \text{sign}(v_c), \tag{15}$$

FIGURE 6: Nonlinear gyrator-capacitor model of a transformer (a) with nonlinear capacitance and resistance and (b) the equivalent circuit using voltage-dependent voltage and current sources.

where v_c is the voltage over the capacitance C_C, and equivalent capacitance

$$C_e(v_c) = \frac{C_c}{1 + a|v_c|^{n-1}}, \tag{16}$$

where C_C represents the core permeance in the linear region, n controls the sharpness of the saturation curve, and a controls the position of the saturation knee.

In addition to the saturation effect, the hysteresis loop is modeled by a nonlinear resistance. This resistance has hyperbolic relationship between voltage and current, hence keeping a nearly constant voltage across its terminals. This is responsible for shifting H and therefore modeling the hysteresis loop. The nonlinear resistance is often represented by a linear resistor in parallel with a voltage-dependent current source defined as

$$I_R(v_r) = b|v_r|^m \operatorname{sign}(v_r), \tag{17}$$

where v_r is the voltage over the resistor r, which leads to an equivalent resistance of

$$R_c(v_r) = \frac{r}{1 + b|v_r|^{m-1}}. \tag{18}$$

Please notice that together the nonlinear capacitor and resistor in the model comprise a nonlinear impedance, which depends on Φ and $d\Phi/dt$ and has memory. Hence, the combination of elements is able to represent the dependency on past states of the magnetic material over the current state. Additionally, the same model is able to represent different types of H-versus-Φ loops, for example, asymmetric loops when current flows in only one direction, loops close to saturation when input voltage is high, or loops without saturation when input voltage is low.

4.2. Parameter Fitting. In this section, the parameters for the nonlinear magnetic behavior of the transformer are shown to be easily determined by an open circuit measurement. In this approach, a sine wave is fed to the primary of the transformer with no load in the secondary. In this case, by observing

Figure 6(a), the open load in the secondary has the effect of a short circuit before the gyrator at H_2, and the effect of leakage inductance C_{l2} of the secondary can be ignored. Hence, Φ and H can be simply obtained from the input current i_1 and the output voltage V_2 measurements via (3) and (1), which are integrated to obtain Φ:

$$H = N_1 i_1,$$
$$\Phi = -\frac{1}{N_2} \int V_2 dt. \tag{19}$$

Once measurements of Φ and H have been obtained, an optimization procedure is needed to determine the nonlinear capacitance and resistance parameters in the model. In the first step, a static saturation model is used to determine the nonlinear capacitance, while the hysteresis effects of Φ and H are ignored. Calculation of the static Φ_s and H_s is performed by determining the center of the hysteresis loop in the Φ versus H curve. Using a nonlinear voltage source model for the nonlinear resistance, it is possible to derive the following Φ and H relationship:

$$\hat{H}_s = \frac{\Phi_s}{C} + a\left|\frac{\Phi_s}{C}\right|^n \operatorname{sign}\left(\frac{\Phi_s}{C}\right), \tag{20}$$

which can be represented in matrix form using the measurement points $\Phi_s[0], \ldots, \Phi_s[K]$ as

$$\hat{\mathbf{H}}_s = \mathbf{\Phi}\alpha, \tag{21}$$

where $\hat{\mathbf{H}}_s$ is a vector with estimated H values for each measurement point k,

$$\mathbf{\Phi} = \begin{bmatrix} \Phi_s[0] & |\Phi_s[0]|^n \operatorname{sign}(\Phi_s[0]) \\ \vdots & \vdots \\ \Phi_s[k] & |\Phi_s[k]|^n \operatorname{sign}(\Phi_s[k]) \\ \vdots & \vdots \\ \Phi_s[K] & |\Phi_s[K]|^n \operatorname{sign}(\Phi_s[K]) \end{bmatrix} \tag{22}$$

represents the matrix containing the measured Φ values, and

$$\alpha = \begin{bmatrix} \dfrac{1}{C} & \dfrac{a}{C^n} \end{bmatrix}^T \tag{23}$$

is a vector with the parameters to be optimized.

Hence, it is possible to define a weighted least-squares solution [27], by using the cost function

$$\xi_a = \left(\mathbf{H}_s - \hat{\mathbf{H}}_s\right)^T \mathbf{W}_a \left(\mathbf{H}_s - \hat{\mathbf{H}}_s\right), \tag{24}$$

where $\mathbf{H}_s$ is a vector with measured H values and $\mathbf{W}_a$ determines the weight each sample has on the optimization process

$$\mathbf{W}_a = \operatorname{diag}\left(\begin{bmatrix} w_{a0} & \cdots & w_{ak} & \cdots & w_{aK} \end{bmatrix}\right). \tag{25}$$
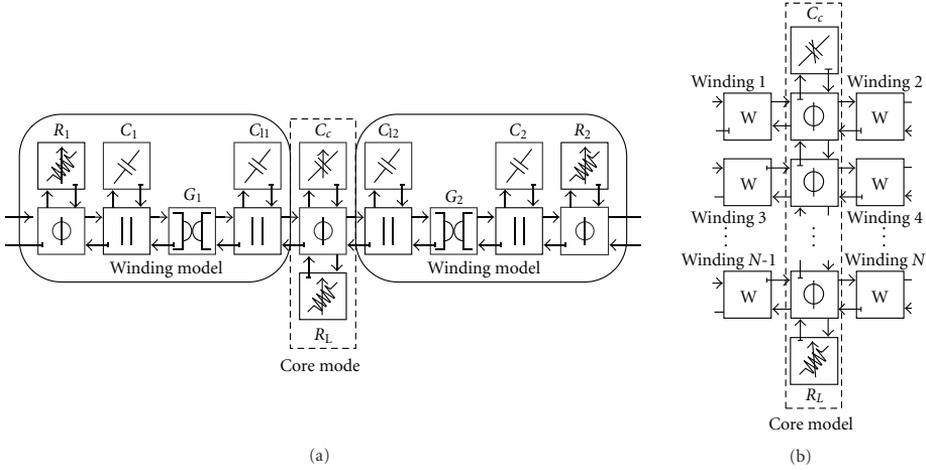
Figure 7: Proposed WDF model of a nonlinear transformer model for (a) two windings and (b) a multiwinding configuration.

By analyzing the gradient of the cost function at $\nabla_\alpha \xi_a = 0$ in

$$\nabla_\alpha \xi_a = \mathbf{H}_s^T \mathbf{W}_a \mathbf{H}_s - 2\alpha^T \mathbf{\Phi}^T \mathbf{W}_a \mathbf{H}_s + \alpha^T \mathbf{\Phi}^T \mathbf{W}_a \mathbf{\Phi} \alpha, \quad (26)$$

it is possible to get the optimum weighted least-squares solution $\hat{\alpha}$ as

$$\hat{\alpha} = \left(\mathbf{\Phi}^T \mathbf{W}_a \mathbf{\Phi} \right)^{-1} \mathbf{\Phi}^T \mathbf{W}_a \mathbf{H}_s. \quad (27)$$

Determination of the parameters, once α is determined, is done as

$$C = \frac{1}{\hat{\alpha}[0]},$$
$$a = \hat{\alpha}[1] C^n. \quad (28)$$

The best value of n is obtained by computing solutions for several n values, and the one with the lowest cost ξ_a is chosen.

Good results are obtained by using a weight w_{ak}, which reduces the solution bias towards high H values and gives more emphasis on the knee part of the Φ versus H curve. Prior normalization of the experimental data may be needed for numerical stability of the matrix inverses in (27).

The nonlinear resistance parameters may be estimated by using the remanence flux density Φ_r or B_r when $H = 0$ as

$$0 = \frac{\Phi_R}{C} + a \left(\frac{\Phi_R}{C} \right)^n + v_R, \quad (29)$$

where v_R is the voltage across the nonlinear resistor when $H = 0$,

$$v_R = \frac{\Phi_r}{C} + a \left(\frac{\Phi_r}{C} \right)^n = r(\dot{\Phi}_R), \quad (30)$$

and the coercive force H_c, when $\Phi = 0$, is

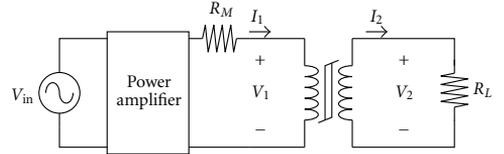$$H_c = v_r = r(\dot{\Phi} + b v_r^m), \quad \Phi = 0, \quad (31)$$

Figure 8: Measurement setup in which the audio transformer is connected to a power amplifier through a series resistor R_M and a load resistor R_L replacing a loudspeaker.

shown in Figure 1 as

$$r = \frac{H_c}{\dot{\Phi}_c - b H_c^m},$$
$$b = \frac{H_c - v_{rc}}{H_c v_{rc}^m - H_c^m v_{rc}}. \quad (32)$$

When no information is available on the number of turns of the transformer, it is possible to use an arbitrary number of turns for the primary and secondary windings with respect to the transformation ratio. This can be easily obtained by fixing N_1 and determining $N_2 = k N_1$. The transformation ratio k can be obtained from the measurements of primary and secondary inductances as $k = \sqrt{L_2/L_1}$.

A practical way to determine parasitic elements is to use a normal commercial multimeter with resistance and inductance measurements. The resistance responsible for ohmic losses is determined by directly measuring each winding resistance. Leakage inductances are determined by measuring the inductance of the winding while short circuiting other windings. Once the leakage inductance L_{lw} for a winding w is determined, the leakage capacitance C_{lw} for the gyrator-capacitor model is determined as
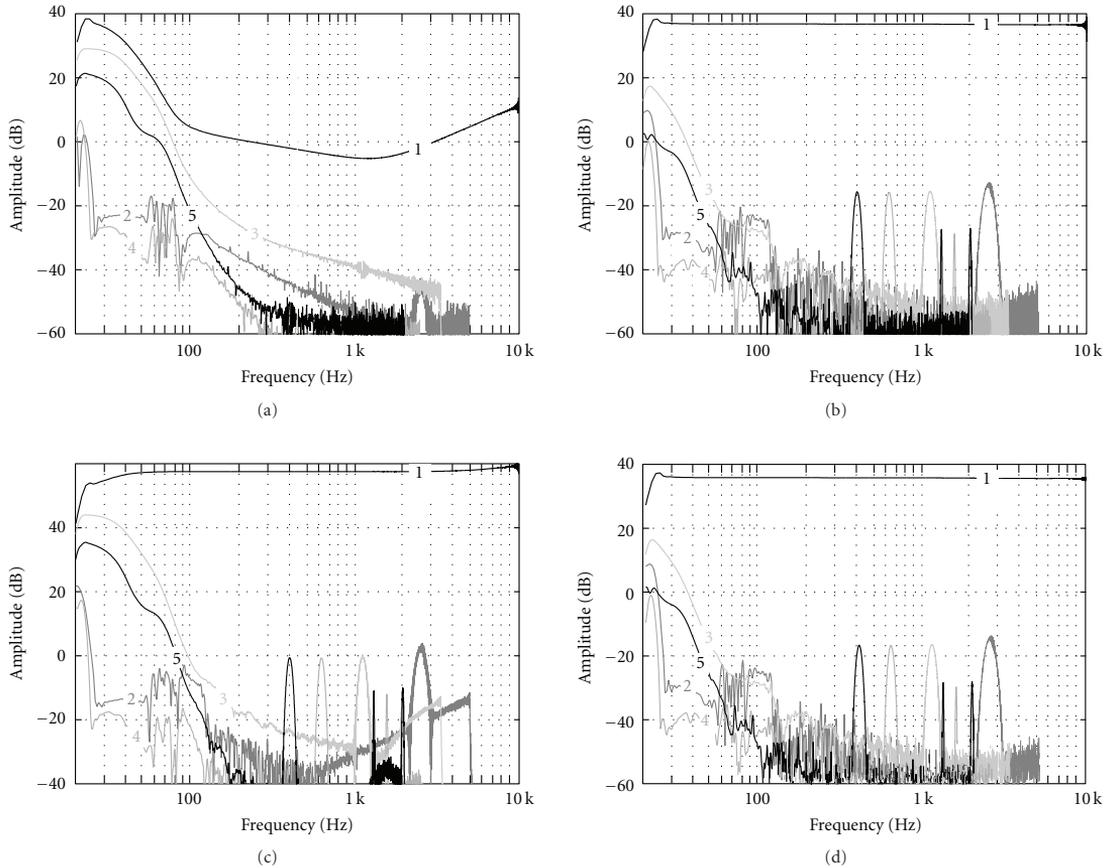
$$C_{lw} = \frac{L_{lw}}{N_w^2}. \quad (33)$$

FIGURE 9: Measurements performed on a Fender transformer using a logarithmic sweep analysis tool [28]: (a) input current, (b) input current with the loaded transformer, (c) output voltage, and (d) output voltage with the loaded transformer. The numbered curves denote the magnitude of each harmonic component, where number 1 refers to the fundamental frequency.

4.3. Wave Digital Filter Model. This section proposes a new WDF model for a two-winding audio transformer in accordance with Figure 7(a). In this model, it is possible to notice common elements for each winding w, which include a gyrator G_w, a capacitor C_{lw} representing the leakage inductance, a capacitor C_w representing winding parasitic capacitance, and a resistor R_w representing ohmic losses. Each winding is connected in series with the nonlinear core elements C_c and R_c.

The nonlinear elements use the approximations described in Section 3. The nonlinear resistor was calculated as in (18), and v_r was delayed by one time sample. The nonlinear capacitance was implemented by using a constant capacitance C_c connected by a nonlinear transformer with the variable turns ratio calculated based on the delayed voltage $v_c = \Phi/C_c$ as

$$N_c(v_c) = \sqrt{\frac{1}{1 + a|v_c|^{n-1}}}. \tag{34}$$

The model in Figure 7(a) can be easily expanded to an N-winding transformer. By connecting each winding's elements in series with the core elements, it is possible to generalize the model for any number of windings, as shown in Figure 7(b). Hence, this model enables a block implementation and easy adaptation for any transformer configuration.

The nonlinear elements in Figure 7 were implemented using delays. This simplification enables connecting several nonlinear elements in the WDF network, without the need for iterations between nonlinear elements.

4.4. Measurement Setup. The practical measurement setup used a Fender NSC041318 transformer, connected to a linear audio amplifier, Yamaha MX-70, as shown in Figure 8. This transformer is commonly used in Fender Deluxe and Deluxe Reverb amplifiers. Since possible output voltages in the power amplifier are often limited, the transformer secondary, which is the low-voltage winding on vacuum tube amplifiers,
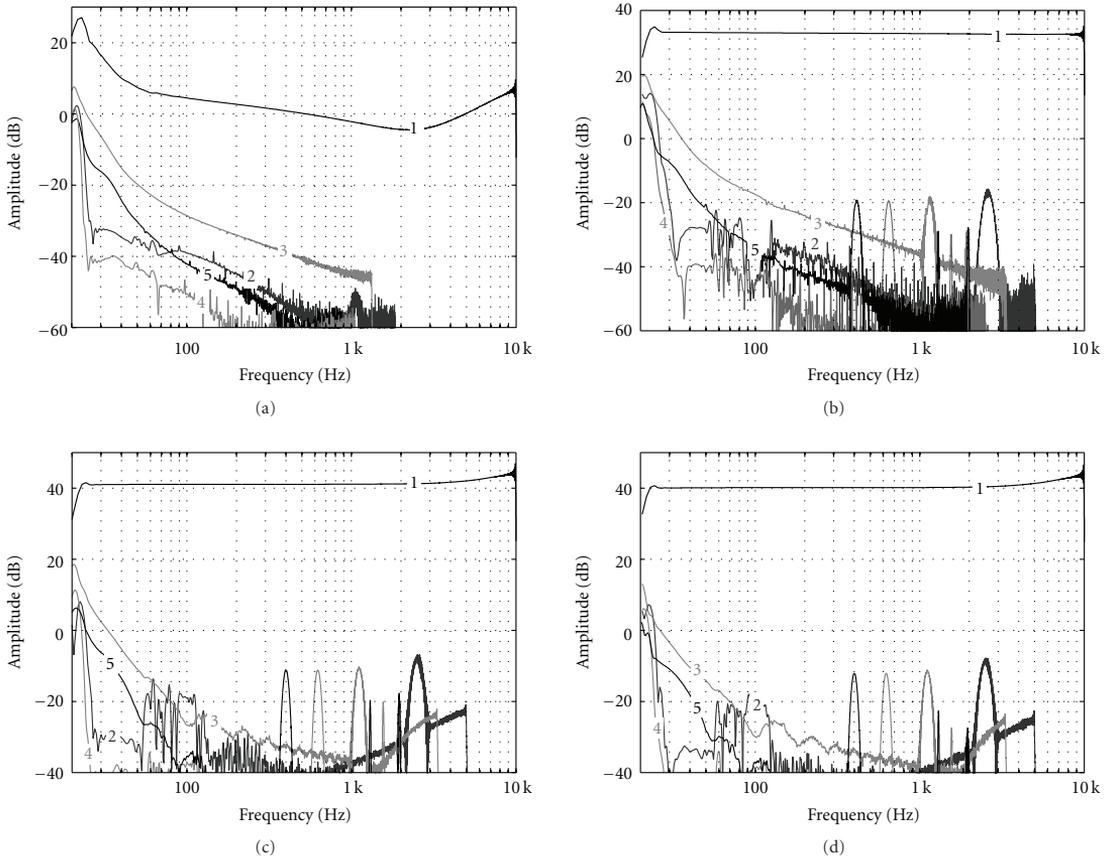
FIGURE 10: Measurements performed on a Hammond transformer using a logarithmic sweep analysis tool [28]: (a) input current, (b) input current with the loaded transformer, (c) output voltage, and (d) output voltage with the loaded transformer. The numbered curves denote the magnitude of each harmonic component, where number 1 refers to the fundamental frequency.

is connected to the power amplifier output. For full load measurements, a load resistor R_L is connected to the high-voltage winding of the transformer. The load resistance value was chosen as

$$R_L = \left(\frac{N_2}{N_1} \right)^2 R_t, \tag{35}$$

where N_1 and N_2 are the primary/secondary number of turns and R_t is the usual loudspeaker resistance, for example, 8 Ω. It is important to notice in practical measurements that resistor R_L will dissipate all of the transformer power during the measurement, and hence a power resistor must be used.

An additional element in the measurement setup includes a series resistance R_M. This is used to measure the input current as well as for limiting the input current if transformer saturation is reached. As shown in Section 2, the transformer impedance is drastically reduced during saturation periods, and hence high current peaks are observed during saturation. The peak limitation is important to avoid

breaking of fuses or other protection mechanisms of the power amplifier during experimental measurements. The input signal for the power amplifier is generated by a computer. This enables either simple analysis using fixed frequency sines or square waves as well as complex analysis, for example, with sweep signals.

Once the transformer was connected, two main sets of measurements were conducted. In the first one, full load was considered with R_L, as in (35), in order to emulate the transformer load when connected to a loudspeaker. In the second set, no load was connected to the transformer primary, or $R_L = \infty$. This open load measurement setup was important to determine the transformer's magnetic elements, as discussed in Section 4.

4.5. Transformer Measurements. Measurements with maximum voltage amplitudes are shown in Figure 9. A logarithmic sweep analysis between 20 Hz and 10000 Hz of the DATK software tool was used [28] for the input current and output
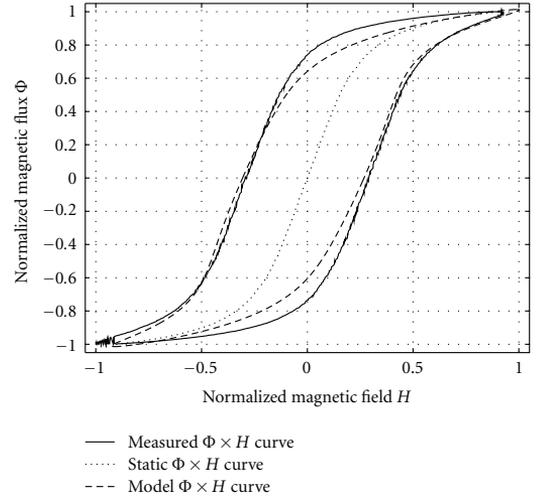
TABLE 1: Parameters used for the Fender transformer model.

Parameter	Value	Unit
N_1	100	—
N_2	6.47	—
C	24.7	mF
a	900	—
n	7	—
r	0.077	Ω
b	4.46	—
m	4	—
C_{l1}	500	nF
C_{l2}	500	nF
R_1	206	Ω
R_2	0.7	Ω
C_1	1	nF
C_2	1	nF

FIGURE 11: Normalized Φ versus H curve for the Fender transformer and model including fitted parameters.

voltage with and without load. In order to avoid current surges during saturation, an input resistance of 2.4 Ω was used, and the input current was measured based on the voltage across this resistor.

The distortion is observed, in Figure 9, to occur at low frequencies, below 100 Hz, since the level of the harmonic components 2–5 generally decays with frequency. By analyzing (1), it is possible to understand that, for the same input voltage, the magnetic flux Φ is larger when the frequency is lower. This explains the strong saturation at low frequencies observed in the results. Comparing the currents and voltages shows that the input current suffers from higher distortion than the output voltage. Hence, it is possible to say that the transformer effect may be in practice enhanced by the interaction between the transformer's changing impedance and the circuitry connected to its primary. Additionally, one sees that the open load input current and the output voltages increase at high frequencies, which indicates the influence of parasitic capacitances, causing a resonance with inductances at high frequencies. The amplitude peaks in Figure 9 for the higher harmonics at high frequencies are due to the measurement artifacts related to the exponential sweep technique and are not present in reality.

Measurements were conducted for two output load situations in order to show that the frequency behavior depends on the type of output load connected to the transformer. Experiments have shown some load dependency on the transformer nonlinearity. By comparing Figures 9(a), 9(c) to Figures 9(b), 9(d), one may observe that by having a resistance as the output load there is a decrease in the harmonic content generated by the transformer's nonlinearity. This is understood by analyzing the equivalent transformer circuit in Figure 6 under short-circuit and open-circuit conditions. In the case of short circuiting the secondary, the small resistance in the secondary of the second gyrator is mapped onto an infinite resistance (or an open circuit) connected in parallel to the capacitor C_{l2}. In the case of an open circuit at the transformer secondary, the infinite resistance is mapped onto a short circuit connected in parallel to the capacitor C_{l2}. Hence, the open circuit case is the one that presents the lowest impedance to the voltage representing the primary magnetizing force H_1, which will cause the highest magnetic flux Φ.

Further measurements were performed for a Hammond T1750V transformer, which is used in the Vox AC30 guitar amplifiers, and the results are shown in Figure 10. It can be seen that this transformer has a lower level of distortion, which is mostly concentrated at very low frequencies, below 30 Hz. When comparing it to the Fender transformer in Figure 9, a lower distortion is observed at all frequencies. Since the normal tuning for the low E string on the guitar is 82.4 Hz (E2), this transformer could be approximated using a linear model.

Parameter fitting of the nonlinear model in Section 4.3 resulted in the values shown in Table 1. The accuracy of the nonlinear model can be observed in Figures 11 and 12. In Figure 11, the Φ versus H curve shows good accuracy for an 80 Hz sine input between the modeled and measured magnetic behavior, which includes both the transformer saturation and the hysteresis. Please notice that these results apply only to the periodic test signals used.

Comparing Figures 12 and 9 shows that the frequency behavior of the model resembles the one observed in practical measurements. The main differences occur in some harmonics that stop decreasing their amplitudes beyond a certain frequency. Those differences may be caused by transformer losses that were not included in the model, such as eddy current losses, which could cause extra energy damping at higher frequencies, as well as inaccuracies in the nonlinear functions for small H and Φ values, since the
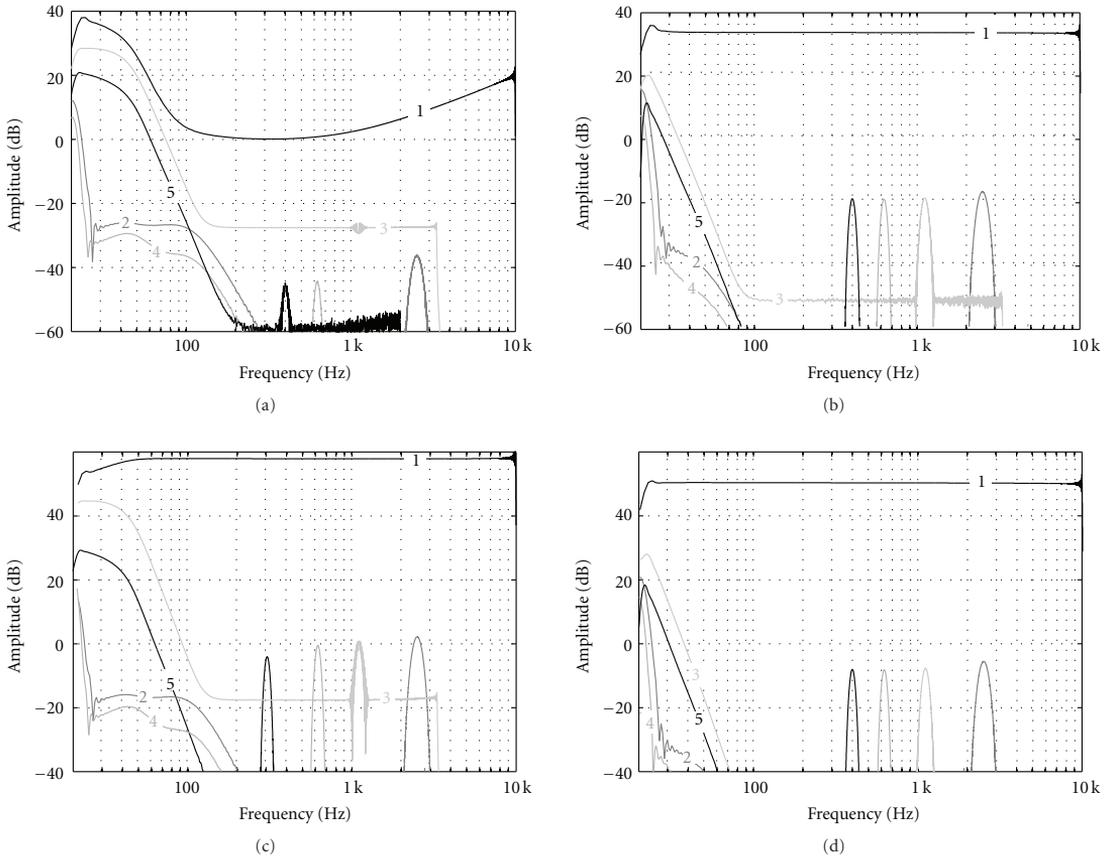
(a)

(b)

(c)

(d)

FIGURE 12: Emulated results with the WDF model based on the Fender transformer using a logarithmic sweep analysis tool [28]: (a) input current, (b) input current with the loaded transformer, (c) output voltage and (d) output voltage, with the loaded transformer. The numbered curves denote the magnitude of each harmonic component, where number 1 refers to the fundamental frequency.

transformer model was optimized for a close-to-saturation condition. Additionally, the high-pass characteristic has differences to the one observed in measured results. This difference can be explained by the fact that in practice the input/output capacitances are distributed throughout the input/output windings. These distributed capacitances could be modeled by several interleaved inductances and capacitances, although this kind of model would significantly increase the computational complexity and make parameter fitting harder.

5. Tube Amplifier Output Chain

This section presents a new complete output chain model for a single-ended vacuum tube guitar amplifier. WDF circuit elements connections are presented in Figure 13(a), which includes a connection to a triode, using Koren's model [29], a linear model for the output speaker shown in Figure 13(b), and the nonlinear transformer model presented in

Section 4.3. The complete circuit is an enhanced version of the single-ended guitar amplifier model presented in [10], while the tube model is the same as that presented in [11].

Simulation results for a sine input are shown in Figure 14. The output sound pressure is measured in this circuit as the current through the loudspeaker acoustic resistance R_a in Figure 13(b). The transformer parameters used in this simulation are the optimized parameters in Table 1, expect for the parameter a, which was modified to provide different levels of transformer distortion.

In the time-domain results shown in Figure 14(a), no transformer saturation is present with $a = 9$, the output signal is a smoothed squared wave, which indicates that distortion results mainly from clipping in the vacuum tube. As the transformer saturation increases, with $a = 90$; the output waveform starts to look like a triangular wave. With $a = 900$, the output transformer is already highly saturated, and the observed output pressure is formed by short impulses.
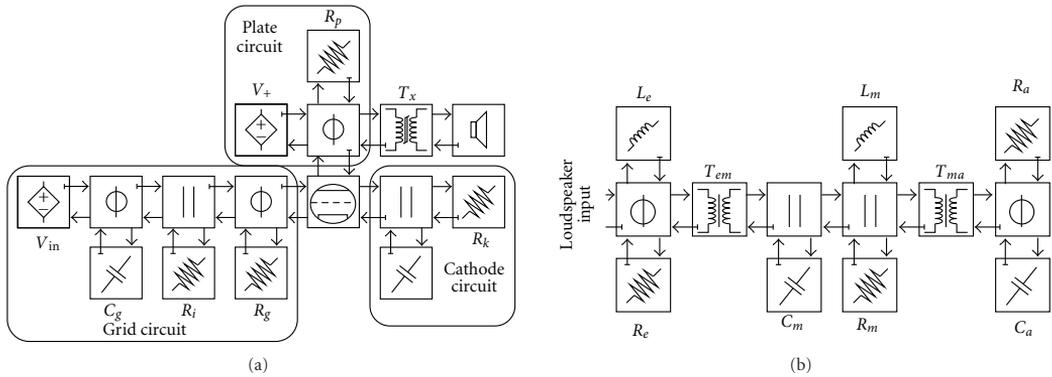
FIGURE 13: WDF implementation of the output chain of a vacuum tube amplifier using the proposed transformer model. (a) The complete circuit and (b) the loudspeaker implementation.
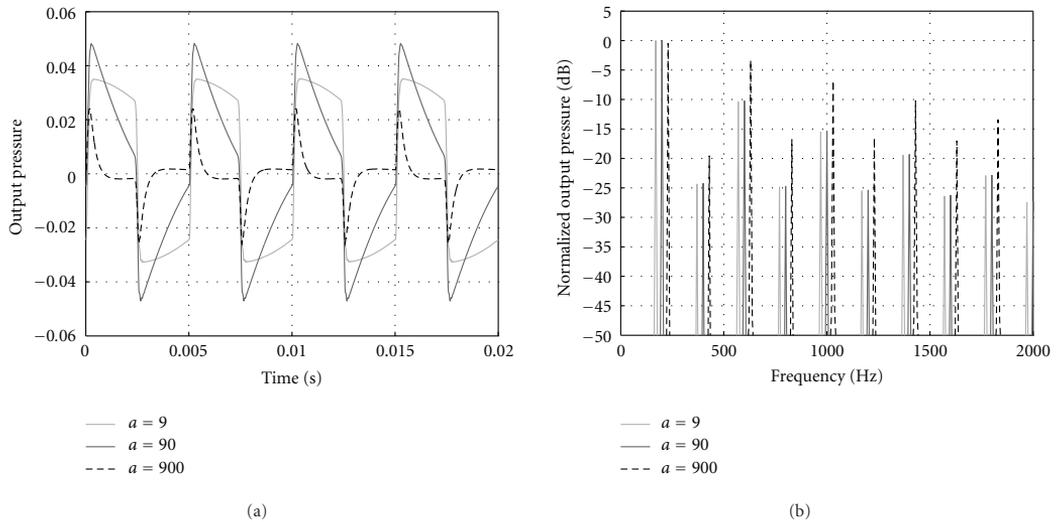

FIGURE 14: Simulated loudspeaker output pressure for different levels of transformer saturation, for an input consisting of a sine with 200 Hz with 3 different levels of transformer saturation in (a) the time domain and (b) the frequency domain. In (b), a frequency offset of 30 Hz is applied for clarity.

In the frequency-domain analysis of the output chain response in Figure 14(b), there are little differences between harmonics for $a = 9$ and $a = 90$. Hence, for a lower transformer saturation, although there would be some differences in the time-domain waveforms, there would be only subtle audible differences. For $a = 900$, there is at least a 5 dB difference for most of the harmonics when compared to $a = 9$. In this case, the transformer saturation contributes to guitar coloration significantly at lower-frequency notes, while little effect should be noticed for higher-frequency notes.

The real-time model is implemented using the BlockCompiler software [30]. Media files will be updated at http://www.acoustics.hut.fi/publications/papers/jasp-trafo/.

The real-time model operates at a 96 kHz sampling rate in a standard PC with an Intel Core 2 Quad CPU, 3 GHz, and 8 GB RAM, and it consumes roughly 7% of CPU time (implementation efficiency improvement is still possible by using other programming languages).

6. Conclusion

A new model for the audio transformer used in tube amplifiers was proposed. Wave digital filters were chosen as the modeling paradigm. The model is based on the previously proposed gyrator-capacitor analogy, in which the nonlinear behavior is represented using voltage-dependent voltage and current sources.

A parameter fitting procedure was introduced. It uses an open circuit measurement in which a sinusoidal input voltage is fed into the primary while there is no load in the secondary. By conducting basic electrical measurements of the input current and output voltage of the audio transformer, the nonlinear capacitance and resistance parameters can be determined. There is no need to know physical parameters of the transformer or even the number of windings. The transformation ratio can be calculated based on the estimated primary and secondary inductances.

As a case study, measurements of a Fender NSC041318 transformer were presented. It was shown that nonlinear distortion is generated mainly at frequencies below about 100 Hz. This implies that audible effects appear only with low guitar tones. A comparison to a Hammond T1750V was made. This transformer presented nonlinear distortion only for frequencies below 30 Hz, which may be inaudible. Once the model parameters were estimated, the WDF model reproduced the behavior of the transformers accurately at low frequencies but not so well at higher frequencies. However, the distortion produced by the model at high frequencies was negligible.

A real-time implementation of the model, which runs in a modern PC at the 96 kHz sample rate, was briefly described. Parameters of the model can be varied freely to change the distortion characteristics. By exaggerating the nonlinearities, a prominent effect, reminiscent of that of the blocking distortion, is obtained.

Future research may look, for example, into the non-linearities of loudspeakers used in guitar amplifiers and the inclusion of frequency-dependent losses in the magnet core of the audio transformer, such as modeling of eddy currents. Additionally, the behavior of the GC model under transient conditions should be evaluated in future studies.

Acknowledgment

References

[1] J. Pakarinen and D. T. Yeh, "A review of digital techniques for modeling vacuum-tube guitar amplifiers," *Computer Music Journal*, vol. 33, no. 2, pp. 85–100, 2009.

[2] T. Hélie, "Volterra series and state transformation for real-time simulations of audio circuits including saturations: application to the Moog ladder filter," *IEEE Transactions on Audio, Speech and Language Processing*, vol. 18, no. 4, pp. 747–759, 2010.

[3] D. T. Yeh, J. S. Abel, A. Vladimirescu, and J. O. Smith, "Numerical methods for simulation of guitar distortion circuits," *Computer Music Journal*, vol. 32, no. 2, pp. 23–42, 2008.

[4] M. N. Gallo, "Method and apparatus for distortion of audio signals and emulation of vacuum tube amplifiers," US patent Application 2008/0218259 A1. Filed on March 2007, published on September 2008.

[5] J. Macak and J. Schimmel, "Nonlinear circuit simulation using time-variant filter," in *Proceedings of the International Conference on Digital Audio Effects*, Como, Italy, September 2009.

[6] D. T. Yeh, *Digital implementation of musical distortion circuits by analysis and simulatio*, Ph.D. thesis, Stanford University, Palo Alto, Calif, USA, 2009, https://ccrma.stanford.edu/~dtyeh/papers/DavidYehThesissinglesided.pdf.

[7] D. T. Yeh, J. S. Abel, and J. O. Smith, "Automated physical modeling of nonlinear audio circuits for real-time audio effects - part I: theoretical development," *IEEE Transactions on Audio, Speech and Language Processing*, vol. 18, no. 4, pp. 728–737, 2010.

[8] M. Karjalainen and J. Pakarinen, "Wave digital simulation of a vacuum-tube amplifier," in *Proceedings of IEEE International Conference on Acoustics, Speech and Signal Processing (ICASSP '06)*, vol. 5, pp. 153–156, Toulouse, France, 2006.

[9] G. De Sanctis and A. Sarti, "Virtual analog modeling in the wave-digital domain," *IEEE Transactions on Audio, Speech and Language Processing*, vol. 18, no. 4, pp. 715–727, 2010.

[10] J. Pakarinen, M. Tikander, and M. Karjalainen, "Wave digital modeling of the output chain of a vacuum-tube amplifier," in *Proceedings of the 12th International Conference on Digital Audio Effects (DAFx '09)*, Como, Italy, September 2009.

[11] J. Pakarinen and M. Karjalainen, "Enhanced wave digital triode model for real-time tube amplifier emulation," *IEEE Transactions on Audio, Speech and Language Processing*, vol. 18, no. 4, pp. 738–746, 2010.

[12] M. Veen and P. Touzelet, "New vacuum tube and output transformer models applied to the Quad II valve amplifier," in *Proceedings of the 114th Audio Engineering Society Convention*, Amsterdan, The Netherlands, March 2003, preprint 5748.

[13] I. Cohen and T. Hélie, "Real-time simulation of a guitar power amplifier," in *Proceedings of the 13th International Conference on Digital Audio Effect (DAFx '10)*, Graz, Austria, September 2010.

[14] J. Macak and J. Schimmel, "Real-time guitar tube amplifier simulation using an approximation of differential equations," in *Proceedings of the 13th International Conference on Digital Audio Effect (DAFx '10)*, Graz, Austria, September 2010.

[15] P. Touzelet, "Accurate non linear models of valve amplifiers including output transformers," in *Proceedings of the 120th Audio Engineering Society Convention*, Paris, France, May 2006, preprint 6830.

[16] D. C. Jiles and D. L. Atherton, "Theory of ferromagnetic hysteresis," *Journal of Magnetism and Magnetic Materials*, vol. 61, no. 1-2, pp. 48–60, 1986.

[17] J. H. Chan, A. Vladimirescu, X. C. Gao, P. Liebmann, and J. Valainis, "Nonlinear transformer model for circuit simulation," *IEEE Transactions on Computer-Aided Design of Integrated Circuits and Systems*, vol. 10, no. 4, pp. 476–482, 1991.

[18] D. C. Hamill, "Gyrator-capacitor modeling: a better way of understanding magnetic components," in *Proceedings of the 9th Annual Applied Power Electronics Conference and Exposition (APEC '94)*, vol. 1, pp. 326–332, February 1994.

[19] Y. S. Lee, L. P. Wong, and D. K. W. Cheng, "Simulation and design of integrated magnetics for power converters," *IEEE Transactions on Magnetics*, vol. 39, no. 2, pp. 1008–1018, 2003.

[20] Q. Chen, L. Xu, X. Ruan, S. C. Wong, and C. K. Tse, "Gyrator-capacitor simulation model of nonlinear magnetic core," in *Proceedings of the 24th Annual IEEE Applied Power Electronics Conference and Exposition (APEC '09)*, pp. 1740–1746, February 2009.

[21] E. D. Torre, *Magnetic Hysteresis*, Wiley-IEEE Press, New York, NY, USA, 1st edition, 1999.

[22] A. Fettweis, "Wave digital filters: theory and practice," *Proceedings of the IEEE*, vol. 74, no. 2, pp. 270–327, 1986.

[23] V. Välimäki, J. Pakarinen, C. Erkut, and M. Karjalainen, "Discrete-time modelling of musical instruments," *Reports on Progress in Physics*, vol. 69, no. 1, pp. 1–78, 2006.

[24] A. Sarti and G. De Sanctis, "Systematic methods for the implementation of nonlinear wave-digital structures," *IEEE Transactions on Circuits and Systems I*, vol. 56, no. 2, pp. 460–472, 2009.

[25] M. Karjalainen, "BlockCompiler documentation," unfinished report, http://www.acoustics.hut.fi/software/BlockCompiler/docu.html.

[26] G. Borin, G. De Poli, and D. Rocchesso, "Elimination of delay-free loops in discrete-time models of nonlinear acoustic systems," *IEEE Transactions on Speech and Audio Processing*, vol. 8, no. 5, pp. 597–604, 2000.

[27] P. S. R. Diniz, E. A. B. da Silva, and S. L. Netto, *Digital Signal Processing: System Analysis and Design*, Cambridge University Press, Cambridge, UK, 2002.

[28] J. Pakarinen, "Distortion analysis toolkit—a software tool for easy analysis of nonlinear audio systems," *EURASIP Journal on Advances in Signal Processing*, vol. 2010, Article ID 617325, 13 pages, 2010.

[29] N. Koren, "Improved vacuum-tube models for spice simulations," *Glass Audio*, vol. 8, pp. 18–27, 1996.

[30] M. Karjalainen, "BlockCompiler: efficient simulation of acoustic and audio systems," in *Proceedings of the 114th Audio Engineering Society Convention*, Amsterdam, The Netherlands, March 2003, preprint 5756.